Hybrid Simulation of a High-Beta Linear Plasma Column Applied with a Low Frequency Wave*)

Takahiro URANO, Toshiki TAKAHASHI, Akiyoshi HOSOZAWA[1)], Tomohiko ASAI[1)] and Shigefumi OKADA[2)]

Graduate School of Science and Technology, Gunma University, Kiryu 376-8515, Japan
[1)]*College of Science and Technology, Nihon University, Tokyo 101-8308, Japan*
[2)]*Osaka University, Suita 565-0871, Japan*

(Received 25 September 2018 / Accepted 13 December 2018)

Wave excitation and propagation by applying a low frequency wave to a high-beta plasma are simulated by a 3-dimensional hybrid model, where ions are treated as particles while electrons are regarded as fluids. It is found that excitation of the toroidal magnetic field occurs outside the separatrix and the wave attenuated significantly near the separatrix. Although the attenuation due to an ion cyclotron resonance is conceivable, no temperature rise in the resonance region is observed. The attenuation condition is given here on the basis of a linear theory, and it shows a good agreement with hybrid simulation results in terms of the attenuation position.

Keywords: high-beta, field-reversed configuration, hybrid simulation, low frequency wave, wave propagation

DOI: 10.1585/pfr.14.2403022

1. Introduction

Field-Reversed Configurations (FRCs) [1] have a closed and an open magnetic field regions which are separated by the boundary that is so-called separatrix. An extremely high-beta plasma is confined inside it. The FRCs' singly connected structure is advantageous because of easier maintenance of confinement structural materials and natural diverter that enables a direct energy conversion of high energy fusion products. Therefore, several conceptual studies of compact fusion reactors have been carried out based on the FRC plasmas [2, 3].

Although the configuration lifetime of the FRC was as short as about several hundreds of microseconds in earlier experiments, the recent FRC researches done at TAE Technology show successful extension of the lifetime by several heating and control techniques, such as NBI [4].

While the lifetime has prolonged, the heating effect by NBI is mainly based on electron heating [5]. Since the temperature equilibration time is longer than that of FRC, ion heating effect is small. For this reason, attention is being paid to a low frequency wave excitation [6–8] as an ion heating technology. The FRC has a field null point inside the plasma, and the resonance surface is narrow because of the high non-uniformity of the magnetic field, and it is said that it is not suitable for wave heating such as ion cyclotron range of frequencies (ICRF) heating. In addition, since the plasma core region has a field-null circle, the plasma size and ion radius are almost comparable. So far, the effect of wave application to the FRC is not clearly understood.

Low frequency wave application to the FRC was studied by Osaka University's FIX device [6, 7]. Excitation of the toroidal magnetic field (B_θ) has been confirmed in the experiment. The measured phase velocity of B_θ suggested the shear Alfvén wave was excited outside the separatrix and the ion acoustic wave inside the separatrix. In addition, an increase in ion temperature was observed by application of the wave. Iwasawa *et al.* analyzed the linear wave propagation considering two-fluid effects for the experiment in the FIX and pointed out the possibility of heating by the transit-time magnetic damping [9].

In order to clarify the characteristics of a low frequency wave applied to an FRC, we carried out a hybrid simulation in which ions in plasma are regarded as particles and electrons are regarded as fluid.

2. Simulation Model

2.1 Target plasma structure and simulation region

A real FRC has a spatial variation in the axial direction, however in our present study we assumed an axially uniform FRC by extending the midplane profile in the axial direction in order to simply analyze the wave applied to the high beta plasma. The plasma shape and the simulation region are shown in Fig. 1. Here, we call this configuration as a high-beta linear plasma column. The equilibrium state is obtained from the Grad-Shafranov equation. The radial distribution of the equilibrium state is shown in Fig. 2. In this simulation, a 3-dimensional (3-d) Cartesian coordinate system is adopted. The reason for this is that generation of numerical noises near the device axis ($r = 0$) is avoided by

author's e-mail: t09306013@gunma-u.ac.jp

*) This article is based on the presentation at the 12th International Conference on Open Magnetic Systems for Plasma Confinement (OS2018).

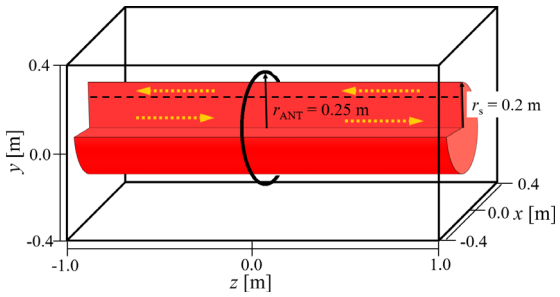

Fig. 1 Plasma shape and simulation region. r_s is separatrix radius. r_{ANT} is antenna radius. The yellow arrow represents the direction of the magnetic field and the black broken line represents the field null point.

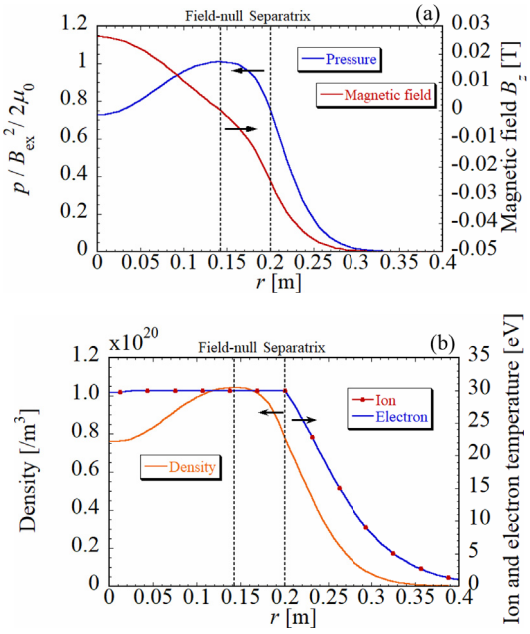

Fig. 2 Radial distributions of (a) plasma pressure p and magnetic field B_z, (b) density n_i, n_e and temperature at equilibrium. Here, B_{ex} is the external magnetic field (0.05 T), μ_0 is the vacuum permeability. Ion (Electron) temperature T_i, T_e = 30 eV, Ion (Electron) density n_i, n_e = 1.05×10^{20} m^{-3}.

employing the Cartesian coordinate system. In addition, the periodic boundary condition is adopted at the device end.

2.2 Calculation model

We performed a 3-d hybrid simulation. Here, ions are treated as weighted super-particles, and electrons are handled as a fluid without mass. We need to take into account the electromagnetic field generated from the antenna. The set of equations including the antenna component is as follows:

$$\mathbf{B}_t = \mathbf{B}_p + \mathbf{B}_{ANT}, \tag{1}$$

$$\mathbf{E}_t = -\mathbf{u}_e \times \mathbf{B}_t - \frac{\nabla p_e}{en_e} + \frac{\mathbf{R}_{ei}}{en_e}, \tag{2}$$

$$-\frac{\partial \mathbf{B}_t}{\partial t} = \nabla \times \mathbf{E}_t, \tag{3}$$

$$\frac{\partial p_e}{\partial t} = -\gamma p_e(\nabla \bullet \mathbf{u}_e) - \mathbf{u}_e \bullet \nabla p_e + (\gamma - 1)\mathbf{R}_{ei} \bullet \frac{\mathbf{j}_p}{en_e} - (\gamma - 1)Q_i, \tag{4}$$

$$\mathbf{j}_p = \frac{1}{\mu_0}\nabla \times \mathbf{B}_p, \tag{5}$$

$$\mathbf{u}_e = \mathbf{u}_i - \frac{\mathbf{j}_p}{en_e}. \tag{6}$$

Here, $\mathbf{B}_t$ is the total magnetic field including the antenna component, $\mathbf{B}_p$ is the magnetic field only of the plasma, $\mathbf{B}_{ANT}$ is that of the antenna, $\mathbf{E}_t$ is the total electric field, $\mathbf{u}_i$ and $\mathbf{u}_e$ are the ion and electron flow velocity respectively, p_e is the electron pressure, e is the elementary charge, n_i and n_e are ion and electron density respectively. In this calculation the charge neutrality $n_i = n_e$ is assumed. The frictional force $\mathbf{R}_{ei}$ is taken into account for the electronic fluid by collision with ions. Further, t is the time, γ is the heat capacity ratio, Q_i is the heat generation term, and $\mathbf{j}_p$ is the plasma current density, respectively. The Runge-Kutta method is used for the time integration of Eqs. (3) and (4). The ion flow velocity and density are obtained by tallying ion particle trajectory calculation results by the PIC method. The equation of motion of ions is

$$m_i \frac{d\mathbf{v}_i}{dt} = q_i(\mathbf{E}_t + \mathbf{v}_i \times \mathbf{B}_t). \tag{7}$$

Here, m_i is the ion mass, $\mathbf{v}_i$ is the ion velocity for individual particles, and q_i is the ion charge. The collision processes are reproduced by the Grid-based coulomb collision model [10]. A time step of particle tracking chosen here is 1/100 of the gyration time at the external magnetic field. Therefore, the ion cyclotron resonance effect is automatically included in the trajectory calculation result.

2.3 Antenna model

Next, the setting of the antenna to excite the wave will be described. We install the antenna as a loop antenna at (r, z) = (0.25 m, 0 m); it is shown in Fig. 1. The antenna current is given by a damped sinusoidal wave with the maximum value of 1 kA and the frequency of 80 kHz. The current waveform is shown in Fig. 3. The maximum value of the magnetic field generated from this antenna current is about 10 mT on the symmetric axis, which is about 1/5 of the external magnetic field.

3. Results and Discussion

The temporal change of the toroidal magnetic field is shown in Fig. 4. Here, we show the time variation of the toroidal magnetic field on the x-z plane at y = 0. In order to observe only the influence by the applied wave, a simulation for no wave application case is done separately.

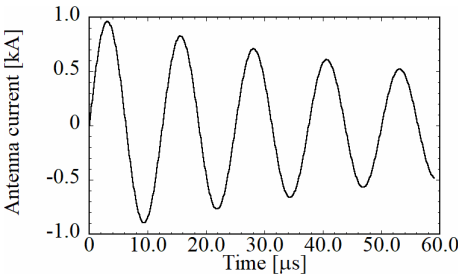

Fig. 3 Waveform of the antenna current.

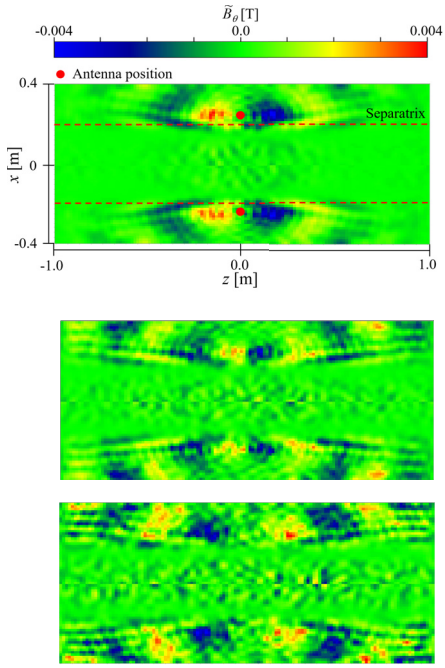

Fig. 4 Temporal change of toroidal magnetic field (antenna frequency 80 kHz), x-z plane ($y = 0$). upper illustration: 10 μs, middle illustration: 20 μs, under illustration: 30 μs. The separatrix position in the figure is the value in the equilibrium state.

The difference in the toroidal field due to the presence or absence of the wave is shown in Fig. 4. Unless otherwise specified, results of such processing are shown and the differences in the magnetic and electric fields are denoted by $\tilde{\mathbf{B}}$ and $\tilde{\mathbf{E}}$ hereafter. From Fig. 4, the toroidal field excited from the vicinity of the antenna mainly propagates in the axial direction with time.

From experiments in the FIX device [6, 7], it is suggested that the shear Alfvén wave

$$v_\phi = \frac{B}{\sqrt{\mu_0 \rho}} \left[1 - (\omega/\omega_{ci})^2\right]^{1/2} \tag{8}$$

is excited outside the separatrix and propagates along the field line. Here, B is the local magnetic field strength, ρ is the ion mass density, ω is evaluated with the antenna frequency ($2\pi f_{ANT}$), and ω_{ci} is the ion cyclotron frequency. On the other hand, the propagation velocity inside the separatrix is in good agreement with the sound velocity of the plasma represented by

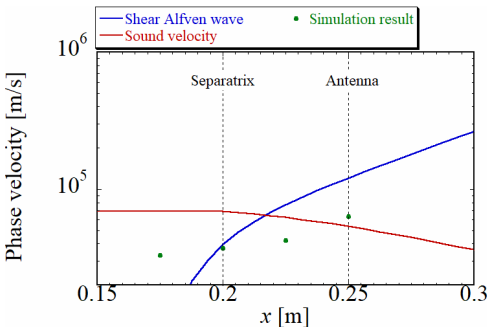

Fig. 5 Axial propagation velocity. The blue line is the shear Alfvén wave and the red line is the sound velocity wave.

$$v_s = \sqrt{\frac{k_B(\gamma_e T_e + \gamma_i T_i)}{m_i}}. \tag{9}$$

Here, k_B is the Boltzmann's constant, $\gamma_{e,i}$ is the specific heat ratio of electrons and ions ($\gamma_{e,i} = 5/3$).

To compare with experimental results, the axial propagation velocity (the direction of the magnetic line of force) of the wave was evaluated from our simulation results. The propagation velocity is obtained from the time until the toroidal magnetic field generated from the antenna reaches the end of the device. It was evaluated at four different radial positions between the inside of the separatrix and the antenna position, and the results are shown in Fig. 5. Note that the radial position on the horizontal axis ranges from the field-null point to the outside of the antenna. For comparison, the profiles of the shear Alfvén velocity and the sound velocity are also shown in Fig. 5. It can be seen that the propagation speed of simulation result is faster outside the separatrix and slower as it approaches the separatrix. The propagation speed of the wave obtained by the simulation is about half as compared with the shear Alfvén velocity and the sound velocity. As for the difference in the phase velocity, we consider that the plasma shape in this simulation are different from the conditions of a real FRC, so it does not necessarily agree with the experimental result.

Next, radial propagation will be discussed. In order to investigate the radial variation of the fluctuation component, the variation in the x direction at $z = 0.25$ m in the toroidal magnetic field is shown in Fig. 6. At any time, it is observed that the amplitude is relatively large outside the separatrix and is small inside. As the amplitude of the excited toroidal magnetic field is decreasing with time, there is a possibility that the energy of the electromagnetic field has been absorbed into the plasma by ion cyclotron resonance. Also, the radial propagation velocity is calculated by obtaining the time from the antenna position to the separatrix until the magnetic field oscillation reached the separatrix, and it is found to be about 20 km/s.

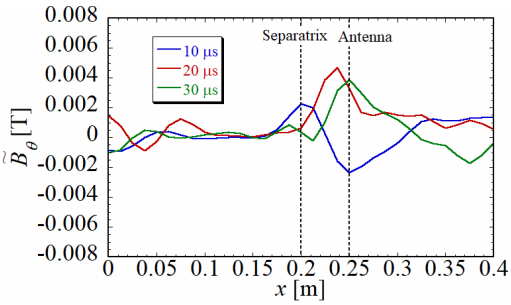

Fig. 6 Radial distribution of toroidal magnetic field at z = 0.25 m (antenna frequency 80 kHz). The separatrix position in the figure shows the position at the equilibrium state.

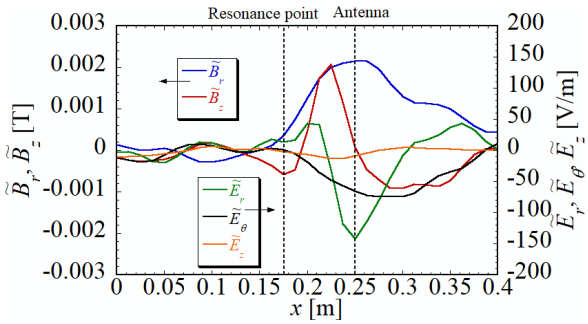

Fig. 7 Radial distribution of electromagnetic field at 10 μs (z = 0.25 m). The resonance point in the figure is calculated from the magnetic field at 10 μs.

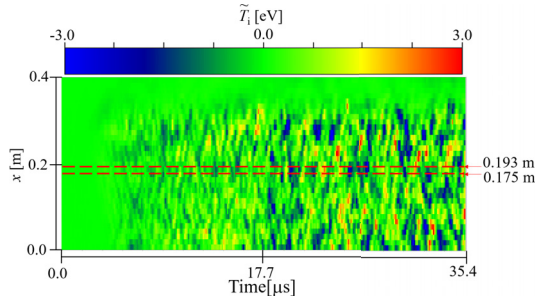

Fig. 8 Temporal change of ion temperature at z = 0.25 m (y = 0 m). Since the magnetic field profile changes with time, the resonance point also changes. The range of the change is indicated by a broken line in the figure.

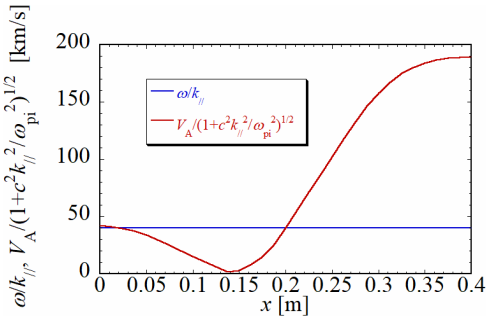

Fig. 9 Relationship between left and right side in Eq. (11).

Figure 7 shows the radial distribution of electromagnetic fields except for $\tilde{B}_\theta$ at 10 μs. The observation point here is the same as in Fig. 6. It is seen that, similarly to $\tilde{B}_\theta$, the amplitude is larger outside x = 0.2 m and smaller on the inner side. From Figs. 6 and 7, the amplitude of the magnetic field is almost the same among the components. The value is about 2 mT, which is about an order of magnitude smaller than the external magnetic field (0.05 T). The amplitude of the electric field varies depending on the component. $\tilde{E}_z$ is small both inside and outside the separatrix This will be explained below. Substituting the electron flow velocity into the equation of the electric field in Sec. 2.2, we obtain

$$\mathbf{E}_t = -\mathbf{u}_i \times \mathbf{B}_t + \frac{\mathbf{j} \times \mathbf{B}_t}{en_e} - \frac{\nabla p_e}{en_e} + \frac{\mathbf{R}_{ei}}{en_e}. \tag{10}$$

In this ideal MHD expression, since the equilibrium magnetic fields B_r and B_θ are zero, E_z is not generated as a linear wave. In other words, we can say that it is relatively close to the ideal MHD model in the vicinity of the antenna outside the separatrix. In addition, we see that the amplitudes decrease at the location slightly outside the resonance point.

The possibility of the ion heating by the ion cyclotron resonance heating will be discussed hereafter. Figure 8 shows the temporal change of ion temperature at z = 0.25 m. The red dashed line gives the range where the time-varying resonance point exists within 35.4 μs shown in Fig. 8. It can be seen that noticeable temperature increase is not seen in the region between the two dashed lines. The ion temperature is only fluctuating, and no increase is found in this region.

Ignoring the dissipation phenomenon in the plasma and linearizing the equation of the hybrid simulation model, when the condition

$$\frac{\omega}{k_{//}} = \frac{V_A}{\sqrt{1 + c^2 k_{//}^2/\omega_{pi}^2}} \tag{11}$$

is satisfied, the fluctuation component of the toroidal magnetic field $\tilde{B}_\theta$ satisfies a condition that does not generate the oscillation of the radial direction component $\tilde{E}_r$ of the electric field. Here, $k_{//}$ is the wave number in the direction of the magnetic force line, V_A is the Alfvén velocity, c is the light velocity, and ω_{pi} is the plasma frequency of the ion. Based on the simulation results, since the wavelength in the region where the amplitude is attenuated is approximately 0.5 m, it can be evaluated as $k_{//} = 4\pi\,\mathrm{m}^{-1}$. Substituting this into Eq. (11), we are able to obtain the relationship shown in Fig. 9. It is found that Eq. (11) is satisfied in the vicinity of the separatrix of x = 0.2 m, which shows that it almost coincides with the attenuation position of the wave.

From this study, we observed the radial distribution of the axial phase velocity of the excited wave. It was also found that the waves propagated in the radial direction attenuated near the separatrix. Although the ion cyclotron resonance has been considered, no rise in ion temperature, however, was observed. As a result of analysis based on linear theory, the condition that the toroidal magnetic field attenuates near the separatrix was suggested.

4. Summary

We have carried out a simulation of applying low frequency wave motion to high beta plasma by using 3 dimensional hybrid simulation model. As a result, it was found that the toroidal magnetic field was excited by the applied low frequency wave, which propagated in the axial and radial directions. The propagation velocity in the axial direction is several tens km/s, and it is faster for larger r. The axial propagation velocity was different from the phase velocity suggested by the FIX device [6, 7]. This disagreement could be due to the inconsistency between the plasma shape of a real FRC and that assumed in this simulation. In the future, we will be a challenge to conduct simulation according to a real FRC. In addition, the excited wave attenuated near the separatrix. The cause was thought to be ion cyclotron resonance, but heating effect was not observed. As a result of analysis based on linear theory, the condition that the excited toroidal magnetic field attenuates near the separatrix was derived. Further deepening analysis by this linear theory is also a future subject.

[1] M. Tuszewski, Nucl. Fusion **28**, 2033 (1988).
[2] H. Momota *et al.*, Fusion Technol. **21**, 2307 (1992).
[3] N. Rostoker *et al.*, Science **278**, 1419 (1997).
[4] H. Guo *et al.*, Nat. Commun. **6**, 6897 (2015).
[5] M. Inomoto *et al.*, Nucl. Fusion **48**, 035013 (2008).
[6] K. Yamanaka *et al.*, Phys. Plasmas **7**, 2755 (2000).
[7] S. Okada *et al.*, Nucl. Fusion **43**, 1140 (2003).
[8] J. Egedal *et al.*, Phys. Plasmas **25**, 072510 (2018).
[9] N. Iwasawa *et al.*, Phys. Plasmas **11**, 615 (2004).
[10] M.E. Jones *et al.*, J. Comput. Phys. **123**, 169 (1996).